Numerical analysis and simulation of the interaction between a Von Kármán vortex street and elastic flaps

Samer Ali, Sébastien Menenteau, Charbel Habchi, Thierry Lemenand, Jean-Luc Harion, Ahmed Elmarakbi

Numerical analysis and simulation of the interaction between a Von Kármán vortex street and elastic flaps

S. ALI[a,b,c], S. MENANTEAU[b,c], C. HABCHI[a], T. LEMENAND[d], J.-L. HARION[b,c], A. ELMARAKBI[e]

a. ETF, School of Engineering, Lebanese International University LIU, P.O. Box 146404 Mazraa, Beirut, Lebanon
b. Université Lille Nord de France, F-59000 Lille, France
c. Mines Douai, EI, F-59500 Douai, France
d. LUNAM Université, Thermofluid Complex Flows and Energy Research Group, LTN CNRS UMR 6607, 44306 Nantes, France
e. Department of Computing, Engineering and Technology, Faculty of Applied Sciences, University of Sunderland, Sunderland SR6 0DD, United Kingdom

Abstract:

The performance improvement of heat exchangers is a major challenge in many industries. Some of these heat exchangers use vortex generators to produce coherent structures that enhance the heat and mass transfer. The aim of this study is to numerically investigate the vortices generated by introducing flexible flaps into an oscillating and laminar flow. More specifically, a square cylinder is inserted into a two-dimensional domain such that a Von Kármán street vortex is generated. The successive wake vortices disrupt a flexible structure that oscillates and produce coherent structures.

The study is performed by numerical simulations. The fluid-solid coupling dynamics and the deformation of the flexible element are simulated using a tool developed with the open source library OpenFOAM. The finite volume method is used to discretize the geometry. The problem is then solved by using the PIMPLE algorithm and a partitioned approach for fluid-structure interaction. The dynamic solver is coupled with a mesh deformation procedure based on Laplace smoothing equation with variable mesh diffusion. The solvers and the coupling method used for modeling fluid-structure interaction are detailed first. The effects of the elastic properties of the flexible structure on the oscillations and the topology of the flow are then investigated.

Keywords: computational fluid dynamics, fluid-structure interaction, Aitken method, OpenFOAM, flexible flap.

1 Introduction

Over the years, many methods have been studied to enhance heat transfer in forced convection problems. A classification of single phase heat transfer enhancement as passive, active, or compound has been proposed by Webb [1]. Active methods require external power and involve electric, magnetic or acoustic fields. Passive methods involve surface modifications, fluid additives or introduction of protuberances in order to destabilize the flow. Compound methods involve the use of both active and passive techniques. Since active methods require external energy and thus an added cost, passive methods are more widely spread in several applications.

Valencia [2] performed a 2D numerical investigation of the unsteady laminar flow pattern and forced convective heat transfer in a channel with a built-in rectangular cylinder. His study shows that oscillatory separated flows result in a significant heat transfer enhancement about a maximum of 45% compared to two-dimensional channel flow. Yang [3] performed a numerical study of heat transfer enhancement in a channel flow using an oscillating vortex generator, the results showed a heat transfer efficiency index greater than 1.0 for almost all cases and in some cases an increment of heat transfer of about 115%.

In the present study, passive oscillating flaps can be obtained without the need of an additional force except the hydrodynamic forces of the flow itself on the flaps. More specifically, a square cylinder is inserted into a two-dimensional laminar flow. Downstream from the square two elastic flaps are inserted. Successive vortices in the wake of the square are produced and disrupt a flexible structure that oscillates and produce coherent vortex structures.

2 Numerical Procedure

A partitioned solver for strongly coupled fluid-structure interaction has been developed using the C++ library OpenFOAM 1.6-ext [4] and validated by Habchi *et al.* [5]. The nonlinear elastic deformation problem is discretized by the method proposed by Jasak and Weller [6]. The internal mesh motion is solved by using the Laplace smoothing equation with variable mesh diffusivity [7].

2.1 Mass, moment and displacement conservation equations

The flow field is governed by mass conservation and Navier-Stokes equations for a laminar viscous incompressible flow. The Arbitrary Lagrangian-Eulerian (ALE) formulation is used to solve the fluid flow [8]. Equations are thus given by:

$$\nabla \cdot \mathbf{u_f} = 0 \tag{1}$$

$$\frac{\partial \mathbf{u_f}}{\partial t} + \left(\mathbf{u_f} - \mathbf{u_{m,f}}\right) \cdot \nabla \mathbf{u_f} = -\frac{\nabla p}{\rho_f} + \upsilon_f \nabla^2 \mathbf{u_f} \tag{2}$$

where $\left(\mathbf{u_f} - \mathbf{u_{m,f}}\right)$ is the convective term. The Eulerian and Lagrangian descriptions are respectively obtained by setting $\mathbf{u_{m,f}} = 0$ or $\mathbf{u_{m,f}} = \mathbf{u_f}$, with $\mathbf{u_{m,f}}$ being the mesh velocity in the fluid domain.

The equations of motion of the elastic structure can be thought from a Lagrangian point of view by:

$$\rho_s \frac{\partial^2 \mathbf{d_s}}{\partial t^2} = \nabla \cdot \left(\mathbf{\Sigma} \cdot \mathbf{F^T}\right) + \rho_s f_b \tag{3}$$

where $\mathbf{d_s}$ is the displacement of the structure, f_b is the resulting body force and $\mathbf{F}$ is the deformation gradient tensor given by:

$$\mathbf{F} = \mathbf{I} + \nabla \mathbf{d_s^T} \tag{4}$$

where $\mathbf{I}$ is the identity matrix.

The spatial discretization of the linear momentum conservation law uses the updated Lagrangian formulation developed by Tucovic and Jasak [10].

2.2 Mesh deformation

In the present study the Laplace smoothing equation is used in order to automatically move the mesh at each time step:

$$\nabla \cdot \left(\gamma \nabla \mathbf{u_m}\right) = 0 \tag{5}$$

where γ is the mesh diffusion coefficient and $\mathbf{u_m}$ is the mesh velocity given by: $\mathbf{u_m} = \left(\mathbf{x}_{t+\delta t} - \mathbf{x}_t\right) / \delta t$, with $\mathbf{x}$ being the mesh position.

It has been shown that less mesh distortion can be achieved by introducing a variable diffusivity in the Laplacian operator. Using the distance-based method, this diffusion coefficient γ is defined as a function of the cell distance to the nearest moving boundary ℓ through the following [7]:

$$\gamma(\ell) = \frac{1}{\ell^2} \tag{6}$$

2.3 Implicit fixed-point coupling

An implicit fixed-point algorithm with dynamic relaxation is used to couple in an accurate way the three solvers (fluid, solid and mesh solvers) and to enforce the equilibrium at the fluid-structure interface [11]. This iterative algorithm is achieved at each time step i at which the fluid and structure fields are solved until fulfilling convergence criterion defined for an outer iteration j. Let $\mathbf{d}^{\Gamma}_{i,j}$ denotes the interface displacement at time step i and outer iteration j. At each time step i and for $j=1$, an interface displacement predictor $\tilde{\mathbf{d}}^{\Gamma}$ is used to improve the convergence and performance of the solver. Then the mesh is moved using the predicted interface displacement as boundary condition, and the new internal mesh motion velocity is obtained and transferred to the fluid flow solver. The fluid flow problem is then solved in ALE formulation using the PIMPLE algorithm for pressure-velocity coupling (a combination of PISO [12] and SIMPLE [13] algorithms). From this point, the pressure and viscous stresses are computed and transferred to the fluid-structure interface as boundary conditions for the solid solver. The solid solver is finally executed to find the predicted displacement $\tilde{\mathbf{d}}^{\Gamma}_{i+1,j+1}$.

3 Computational domain and test case configurations

The computational domain consists of a fixed square cylinder inserted in a two-dimensional channel followed by two elastic flaps, sharing a common rigid base as shown in FIG. 1. It is to be noted that the square cylinder is slightly translated to one side of the channel so that the wake vortices will impact the two flaps in a non symmetrical way. Both flaps have a height h of 50 mm with a thickness of 3 mm, and the cylinder have a width D of 20 mm.

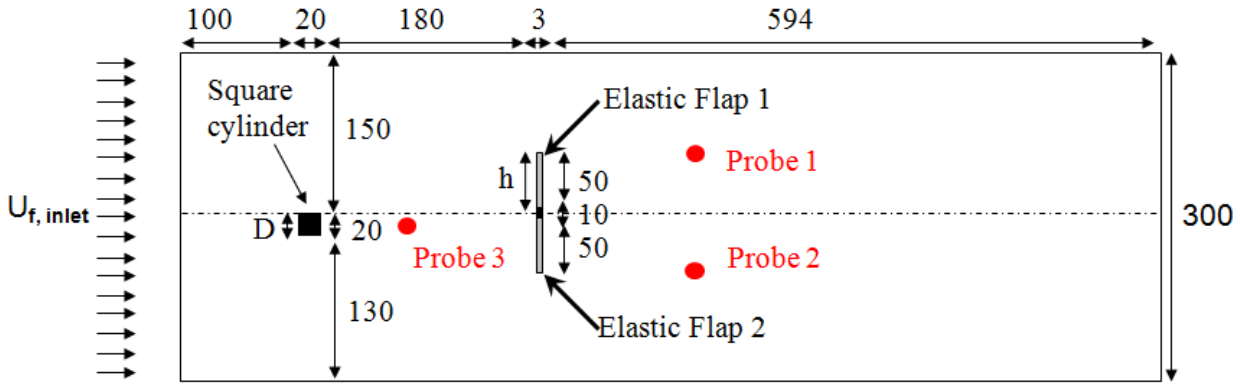

FIG. 1 - Schematic view of computational domain with mm as unit of length

The lateral walls are set as symmetry planes. The outlet condition is set as zero pressure gradient. The inlet velocity profile is considered to be uniform with a velocity of 0.6 m/s with a smooth increase of velocity during the first time steps to avoid a sudden impact on the elastic structures:

$$U_{f,inlet} = 0.6\left[1-\cos\left(\frac{\pi}{2}t\right)\right] \quad for\, t < 0.5\,\mathrm{sec} \tag{7}$$

$$U_{f,inlet} = 0.6\ m/s \quad for\, t \geq 0.5\,\mathrm{sec} \tag{8}$$

where $U_{f,inlet}$ is the fluid inlet velocity.

Three different cases are studied with the same flow configuration (kinematic viscosity, $\nu_f = 5.10^{-5}$ $m^2 s^{-1}$, density $\rho_f = 1$ kg m^{-3}). The Reynolds number based on the height of a flap, $Re_h = U_{f,inlet}\, h / \upsilon_f$ is 600 while the Reynolds number Re_D, based on the width of the cylinder, is 240. As far as the flaps are concerned, one configuration has been set with rigid flaps while the two others have flexible flaps with different Young's modulus values, as reported in

.

In this paper the fluid domain consists of 22044 quadrilateral cells refined at the walls and at the fluid structure interface. The structural domain consists of 2000 quadrilateral cells.

Parameters	Rigid Flap Case: RF	Flexible Flap Case 1: FF1	Flexible Flap Case 2: FF2
ν_s	-	0.4	0.4
ρ_s (kg m^{-3})	-	400	400
E (10^5 Pa)	-	1	0.5

Table 1: Parameters of the flaps stiffness

4 Results: flow pattern and flap oscillations

4.1 Flow pattern

In order to highlight the coherent structures generated in both rigid and flexible flaps cases, snapshots of λ_2 criterion are depicted in FIG. 2 at two time steps taken after the flow stabilization in the RF and FF1 cases.

The λ_2 definition corresponds to the pressure minimum in a plane, when contributions of unsteady irrotational straining and viscous terms in the Navier-Stokes equations are discarded; it is the median of the three eigen values of $S^2+\Omega^2$, where S and Ω are respectively the symmetric and antisymmetric parts of the velocity gradient tensor $\nabla\mathbf{u}$. The vortices are thus characterized by positive values of the -λ_2 criterion and can easily be detected. It is to be noticed that a Von Kármán vortex street occurs behind the fixed square cylinder with a shedding frequency of $f \approx 4.5$ *Hz*. The frequency is determined by performing a Fast Fourier Transformation on velocity oscillations computed at the probe 3 location behind the square cylinder, as shown in FIG. 1. This frequency corresponds to a Strouhal number of *St=0.15*, calculated based on the square width $S_t = \frac{fD}{U_{f,inlet}}$. This wake region then disturbs the flaps located downstream in a non symmetrical way. In FIG. 2, although the flaps are oscillating due to the upstream flow, it is unclear whether the mixing is enhanced with the flexible flaps from the λ_2 criterion visualization.

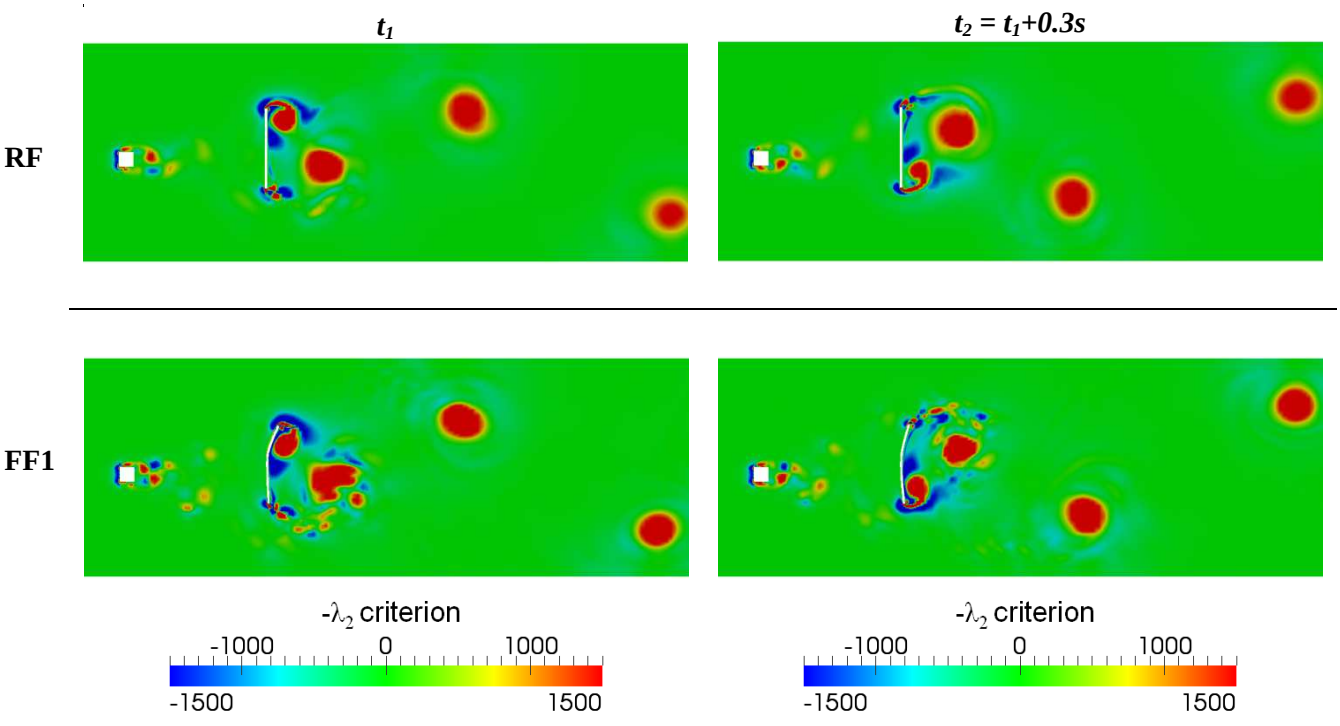

FIG. 2 - Snapshots of -λ_2 criterion for RF case (top figures) and FF1 (bottom figures) – Time step t_1 (left figures) has been arbitrary set and $t_2 = t_1+0.3s$ (right figures)

4.2 Effect of elasticity

In FIG. 3 relative displacement of each flap for the two cases corresponding to different Young's modulus is plotted (see

). FIG. 4 shows a sample comparison where flow velocity magnitude is displayed behind flap 1 for FF2 and RF cases.

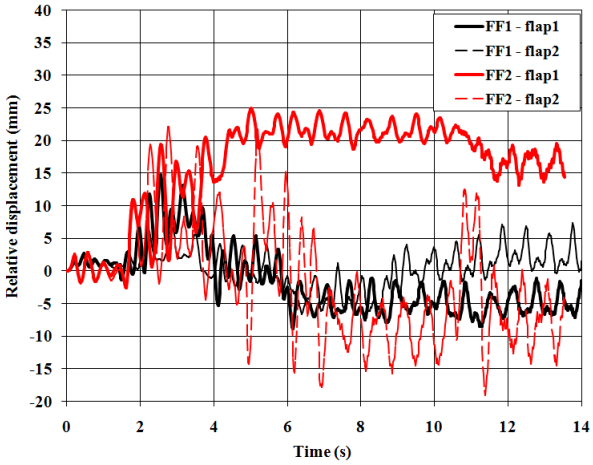

FIG. 3 - Relative displacements of flaps as a function of time for FF1 and FF2 cases

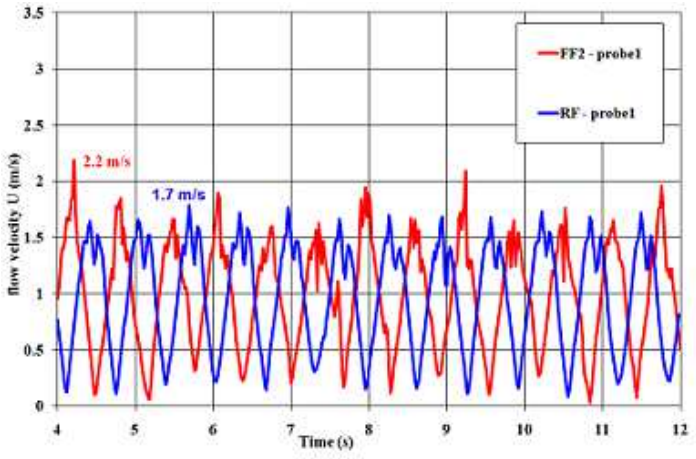

FIG. 4 - Flow velocity as a function of time at probe 1 location behind flap 1, for FF2 and RF cases

In FIG. 3, the mean relative displacement of flap1 increases from -1.63 mm in FF1 case to 16.1 mm in FF2 case, and the mean relative displacement of flap2 increases from 0.36 mm for FF1 to -1.66 mm for FF2, as the Young's modulus decreases from 1×10^5 Pa to 0.5×10^5 Pa. It seems that oscillations of both flaps in both cases have stabilized after 12 seconds, but more time steps are required in order to verify whether oscillations are self-sustained.

Cases		Flap maximum amplitude (mm)	Mean flow velocity (m/s)	Standard deviation	Minimum flow velocity (m/s)	Maximum flow velocity (m/s)
FF1	probe1	-8.55	0.48	0.413	0.005	1.656
	probe2	7.07	0.93	0.438	0.090	1.763
FF2	probe1	24.04	0.99	0.464	0.035	2.200
	probe2	-19.07	0.97	0.373	0.104	1.780
RF	probe1	-	0.96	0.462	0.083	1.727
	probe2	-	0.93	0.374	0.202	1.598

Table 2: Flap and flow parameters for the three cases computed at probe 1 and probe 2.

Table 2 shows that mean velocity increases from 0.48 m/s to 0.99 m/s and from 0.93 m/s to 0.97 m/s as the flap amplitude are higher in the flexible case FF2 than in FF1. Moreover FF2 displays higher mean velocity values than the rigid case (RF), as mean velocity increases from 0.96 m/s to 0.99 m/s and from 0.93 m/s to 0.97 m/s. It is worthy to notice that the maximum flow velocities for flexible cases are higher than for rigid

cases with an increase up to 30%, from a maximum of 1.7 m/s in the rigid case to a maximum of 2.2 m/s in the elastic case as shown in FIG. 4.

After 12 seconds, when oscillations of flaps seem to stabilize, flap 2 for example reaches a lock-in frequency between flap oscillation frequency and shedding frequency at probe 1 with an approximate value of 1.5 Hz.

5 Conclusion

The coupled fluid-structure numerical simulations have been carried out using an in-house partitioned code developed using the open source C++ library OpenFOAM. The fluid flow is solved via an Arbitrary Lagrangian-Eulerian (ALE) formulation and the solid deformations are computed by taking into account large structural deformation and strong coupling between the flow and the elastic solid, performed by an adaptive iterative method using Aitken under-relaxation parameter.

The studied case consisted of two elastic flaps inserted at the median of a channel flow. The flaps oscillate in a passive way without additional external source as a vortex shedding behind a fixed square cylinder perturbed the upstream flow of the flaps. One configuration with rigid flaps is compared to two configurations with flexible flaps with varying Young modulus values. As main conclusions, flexible flaps cases resulted in higher amplitude of velocity oscillations in the wake region of the flaps, with an increase of velocity up to 30% for case FF2. Amplitudes of oscillations are thus found to be larger with reduced elasticity of the flaps. Eventually, vortices created by each flap are shown to induce disturbances of the motion on the adjacent flap, thus raising the chance of the oscillations to be self-sustained.

References

[1] Webb R.L., Enhancement of Single-Phase Heat Transfer, New York, Wiley Interscience, 1987.
[2] Valencia A., Heat transfer enhancement in a channel with a built-in rectangular cylinder, Heat and Mass Transfer, 30, 423-427, 1995.
[3] Yang S.-J., Numerical study of heat transfer enhancement in a channel flow using an oscillating vortex generator, Heat and Mass Transfer, 39, 257-265, 2002.
[4] *OpenFOAM, The Open CFD Toolbox - User Guide, 2013*
[5] Habchi C., Russeil S., Bougeard D.,. Harion J.-L, Lemenand T., Ghanem A., Partitioned solver for strongly coupled fluid–structure interaction, Computers & Fluids, 71, 306-319, 2013.
[6] Jasak H.and Weller H.G., Application of the finite volume method and unstructured meshes to linear elasticity, International Journal for Numerical Methods in Engineering, 48, 267-287, 2000.
[7] Jasak H. and Tukovic Z., Automatic mesh motion for the unstructured finite volume method, Trans FAMENA, 30, 1-18, 2007.
[8] Donea J., Huerta A., Ponthot J.-Ph., Rodriguez-Ferran A., Arbitrary Lagrangian–Eulerian Methods, Encyclopedia of Computational Mechanics, 1, JohnWiley & Sons, Ltd, 2004.
[9] Bos F.M., Numerical simulations of flapping foil and wing aerodynamics, PhD, Technical University of Delft, Netherlands, 2010.
[10] Tukovic Z., Jasak H., Updated lagrangian finite volume solver for large deformation dynamic response of elastic body, Transaction of FAMENA, 31, 1-16, 2007.
[11] Küttler U. and Wall W.A., Fixed-point fluid–structure interaction solvers with dynamic relaxation, Computational Mechanics, 43, 61-72, 2008.
[12] Issa R.I., Solution of the implicitly discretised fluid flow equations by operator-splitting, Journal of Computational Physics, 62, 40-65, 1985.
[13] Patankar S.V.and Spalding D.B., A calculation procedure for heat, mass and momentum transfer in three-dimensional parabolic flows, International Journal of Heat and Mass Transfer, 15, 1787-1806, 1972.